The Distributed Edge Dipole (DED) Model for Cabinet Diffraction Effects*

M. URBAN, C. HEIL, C. PIGNON, C. COMBET, AND P. BAUMAN, *AES Member*

L-ACOUSTICS, 91462 Marcoussis, France

A simple model is proposed to account for the effects of cabinet edge diffraction on the radiated sound field for direct-radiating loudspeaker components when mounted in an enclosure. The proposed approach is termed the distributed edge dipole (DED) model since it is developed based on the Kirchhoff approximation using distributed dipoles with their axes perpendicular to the baffle edge as the elementary diffractive sources. The DED model is first tested against measurements for a thin circular baffle and then applied to a real-world loudspeaker that has a thick, rectangular baffle. The forward sound pressure level and the entire angular domain are investigated, and predictions of the DED model show good agreement with experimental measurements.

0 INTRODUCTION

The frequency response and directivity of a loudspeaker system depend on the shape of the baffle, the location of the sound source on the baffle, and the directivity of the sound source itself. Olson [1] was the first to present experimental results concerning cabinet edge diffraction, observing that the radiated sound field depends on the geometry of the baffle.

Bews and Hawksford (B&H) [2] used the geometric theory of diffraction to model diffraction due to the baffle edges. In their approach, sound rays propagate along the surface of the baffle and are scattered by the edges, producing a series of infinitesimal omnidirectional secondary edge sources.

Vanderkooy [3] derived an angular form factor for the edge sources using Sommerfeld diffraction theory. The diffracted pressure is no longer omnidirectional and is highly dependent on the projected angle of observation. Vanderkooy's experimental results concerning the phase behavior of the edge diffraction wave are highly significant and of great interest.

However, current literature concerning the phenomenon of edge diffraction is somewhat contradictory, and Wright provides an excellent summary of the major inconsistencies [4]. Wright relies on finite-element analysis to consider cabinet edge diffraction, and his modeling results are corroborated by practical experiments. Wright's findings are very important for the development of the DED model, as will be discussed in the following.

Fig. 1 shows a representation of the baffle edge diffraction geometry, which is common to all models outlined in

[4]. The sound pressure from the source P_{drive} propagates to the baffle edges where it energizes a diffractive edge sound source. The sound pressures of the driving source and the contribution of the edge sources must be added in order to determine the sound pressure at a given observation point. Essentially the problem is to characterize the radiated sound field due to the edge sources or to determine an equivalent type of sound source that will account for edge-related diffraction effects.

In this paper we choose to express the driving sound pressure for a piston mounted on a finite baffle as follows:

$$P_{\text{drive}}(r, \theta) = K(\theta)\, P_{\infty\text{baffle}}(r, \theta) \tag{1}$$

where

$P_{\infty\text{baffle}}(r, \theta)$ is the sound pressure produced by the piston when situated on an infinite baffle, $K(\theta)$ is an angular form factor for the driving sound pressure, which is characteristic of a given model, and θ is the polar angle between the direction of observation and the axis of the source.

The elementary pressure induced by the edge sources can be expressed as

$$dP_{\text{edge}}(r, \theta) = F(\theta)\, P_{\text{drive}}(r = L, \theta = 90°)\, \frac{e^{-jkr_P}}{2\pi\, r_P}\, dl. \tag{2}$$

$$P_{\text{edge}} = \oint_{\text{around edge}} dP_{\text{edge}} \tag{3}$$

where

L	distance from piston center to edge element projected differential length along baffle edge, $dl = L\, d\phi$
r	distance from piston center to observation point

r_P distance from edge element to observation point
$F(\theta)$ angular form factor for edge sources; characteristic of a given model.

The resultant pressure at the observation point is obtained by adding the driving and edge contributions,

$$P_{\text{total}}(r, \theta) = P_{\text{drive}}(r, \theta) + P_{\text{edge}}(r, \theta). \tag{4}$$

As a basis for comparison, the B&H [2] and Vanderkooy [3] models will be evaluated. It will be seen that the forward sound pressure level (SPL) as a function of frequency is described correctly by these two models. However, both of these approaches are inaccurate when it comes to characterizing the angular SPL dependence, and this is especially true at $\theta = 90°$.

Section 1 presents the models from [2] and [3], introduces the DED model, and compares all three modeling approaches. In Section 2 a point source mounted on a finite baffle is analyzed using the DED model and following this, the case of an extended sound source is considered. In Section 3 the adopted experimental procedure is described, and in Section 4 a detailed comparison of the predictions of all three models is presented, with experimental data for a thin circular baffle. Finally in Section 5 a more realistic thick, rectangular boxlike cabinet is measured and compared to the predictions of all three models.

1 DESCRIPTION AND COMPARISON OF THREE MODELING APPROACHES FOR CABINET EDGE DIFFRACTION

Fig. 2 defines the wedge angle θ_W and the boundary between shadow and illuminated zones. The wedge angle is defined by considering a section view along the edge of the baffle. The angle ψ is the angle necessary to turn around the baffle completely, and the wedge

angle is defined as the interior angle of the baffle, that is, $\theta_W = 2\pi - \psi$.

Fig. 2 shows two different baffle types. One is very thin and corresponds to a wedge angle of 0° whereas the other is boxlike with a wedge angle of 90°. Both baffle types will be studied experimentally.

The dashed line extending along SP represents the geometric shadow boundary. A straight line going from the sound source to an observer situated in the shadow region will have to pass through the baffle.

1.1 Driving Pressure in Shadow Zone

For a finite baffle it is possible to have an observation point in the shadow region so the driving pressure must be defined there. The question that arises is: should the driving pressure for the shadow region be symmetrical to the driving pressure in the illuminated region, that is, for $\theta > 90°$, $P_{\text{drive}}(\theta) = P_{\text{drive}}(180° - \theta)$, or should it be zero and therefore introduce a discontinuity on the boundary? Different driving pressure formulations in the shadow zone are discussed in the following section for the various modeling approaches.

1.2 Description of B&H and Vanderkooy Models

For B&H [2] there is no indication as to what the driving pressure should be in the shadow region. Since B&H do not consider more than 10° off axis, consequently their angular form factor for the driving sound pressure is set to $K_{\text{BH}}(\theta) = 1$ ($\theta \le 90°$).

Vanderkooy [3] assumes that the driving pressure is zero in the shadow region and the sound pressure in this region is due to radiation from the baffle edges only. We thus have $K_V(\theta) = 1$ for $\theta \le 90°$, and $K_V(\theta) = 0$ for $\theta > 90°$ for the Vanderkooy model.

1.2.1 Elementary Edge Diffraction Sources

The B&H model assumes that each elementary edge element is sending out an isotropic spherical wave in phase opposition with the main piston. Therefore the B&H
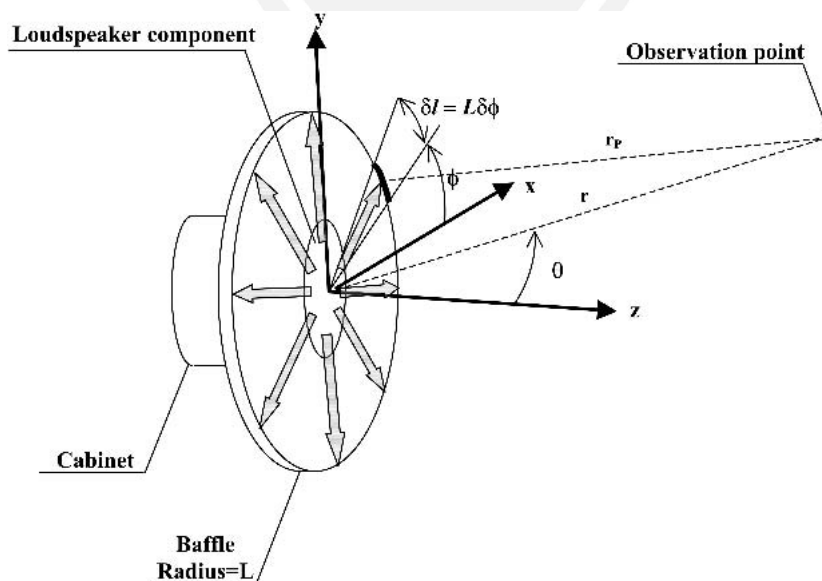

Fig. 1. Geometry common to all approaches for characterizing baffle edge diffraction.

angular form factor for the edge diffraction sources can be written as

$$F_{BH}(\theta) = F_{BH} = \left(\frac{4\pi}{4\pi - 2\theta_W} - 2 \right) \frac{1}{2}. \tag{5}$$

Vanderkooy considers elementary edge sources with an angular dependence that has phase opposition in the forward direction and is in phase toward the rear. In general, the Vanderkooy angular form factor for the edge diffraction sources can be expressed as

$$F_V(\chi)$$
$$= \frac{1}{2} \frac{\sin[\pi^2/(2\pi - \theta_W)]}{1 - \theta_W/2\pi} \frac{1}{\cos\left(\dfrac{\pi}{2 - \theta_W/\pi} \right) - \cos\left(\dfrac{\chi}{2 - \theta_W/\pi} \right)}. \tag{6}$$

The Vanderkooy angular form factor is now developed for a thin circular baffle. In Fig. 3 M runs along the circular baffle and represents the edge element. The position of M is defined by the angle ϕ, which runs from 0 to 2π, and the radius $OM = L$. A distant observation point P is shown in Fig. 3 and the vector OP makes an angle θ with OZ. P' is the projection of P onto the plane $X'OZ$, and χ is the angle between MO and MP'.

For a thin baffle the wedge angle $\theta_W = 0°$ and the expression for $F_V(\chi)$ reduces to

$$F_V(\chi) = \frac{-1}{2\cos(\chi/2)}. \tag{7}$$

Two cases exist for the shadow and illuminated zones,

$$(\chi < \pi) \Rightarrow F_V(\chi) = -\frac{1}{2} \sqrt{\frac{2}{1 + \cos\chi}}$$

$$(\chi > \pi) \Rightarrow F_V(\chi) = \frac{1}{2} \sqrt{\frac{2}{1 + \cos\chi}} \tag{8}$$

and since

$$\cos\chi = \frac{MO \cdot MP'}{MO\ MP'} = \frac{MO^2 + MO \cdot OP'}{MO\ MP'}$$
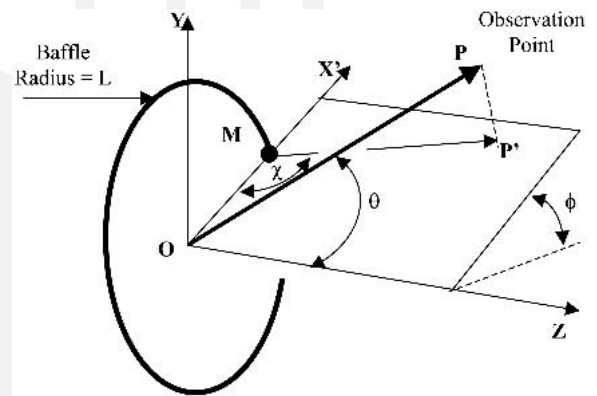

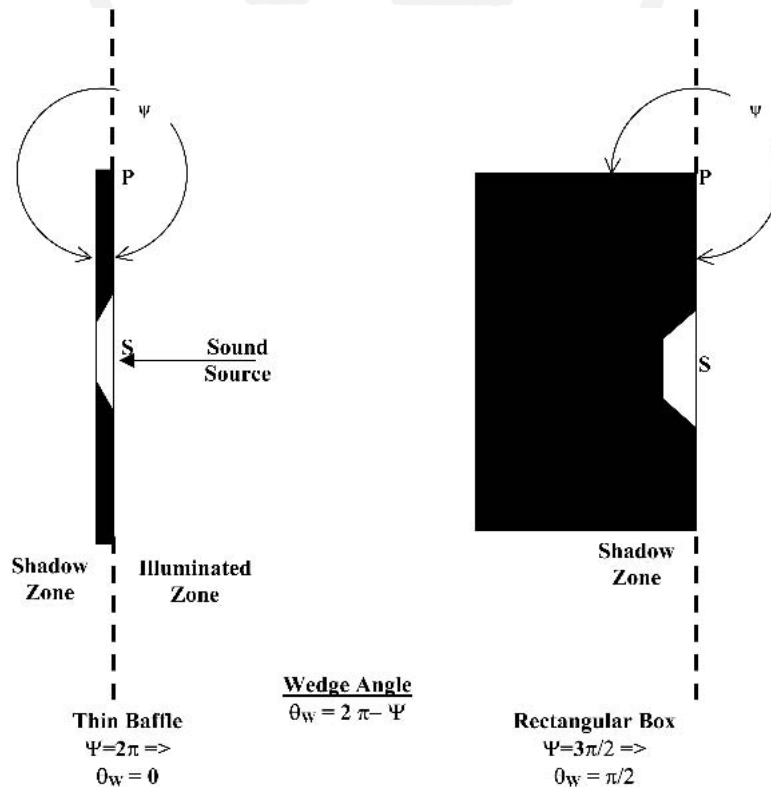Fig. 3. Geometry used to calculate angular form factor for Vanderkooy model.

Fig. 2. Description of wedge angle θ_W and shadow and illuminated zones for two kinds of baffles studied.

the angular form factor F_V for Vanderkooy can be written as

$$F_V(\chi) = F_V(\theta, \phi)$$

$$= \frac{1}{2} \frac{-\sqrt{2}}{\sqrt{1 + \dfrac{L - OP \sin\theta \cos\phi}{\sqrt{(OP \sin\theta \cos\phi - L)^2 + (OP \cos\theta)^2}}}}. \quad (9)$$

1.3 Description of DED Model

An experiment described in [3] served as the conceptual basis for the DED model. The experimental setup consisted of a circular, 1-m-diameter wooden disk with a tweeter mounted at its center. An electric impulse was applied to the tweeter and the pressure response was measured at a 1-m distance, either directly on the tweeter axis or behind the disk. It was observed that the wave radiated from the edges was in phase opposition when facing the baffle (illuminated zone) and in phase when the observation point was behind the baffle (shadow zone).

This experimental result prompted us to visualize the phenomenon in the following way. When the main piston compresses the air at very low frequencies, the air flows in every direction and, in particular, along the baffle surface until it reaches the edge, turns around, and goes behind. This movement of the air around the edge is like a "ring piston" moving backward in opposition to the main piston. It is thus possible to understand the "phase reversing" in the illuminating zone and the "in-phase" pressure in the shadow zone. In an attempt to further describe this ring piston effect the following is shown in the Appendix, using the Kirchhoff approximation.

1) The driving pressure for a source mounted in a finite baffle versus an infinite baffle becomes

$$P_{\text{drive}}(r, \theta) = P_{\infty\text{baffle}}(r, \theta) \frac{1 + \cos\theta}{2}$$

$$\Rightarrow K_{\text{DED}}(\theta) = \frac{1 + \cos\theta}{2}. \quad (10)$$

2) The ring piston can be described as a distributed dipole source,

$$P_{\text{edge}}(r, \theta) = -\cos\theta \, P_{\text{drive}}(r = L, \theta = 90°) \int_0^{2\pi L} \frac{e^{-jkr_P}}{2\pi r_P} \, dl$$

$$\Rightarrow F_{\text{DED}}(\theta) = -\cos\theta. \quad (11)$$

The cosine term in Eq. (11) is a signature of dipole behavior. The axis of the dipole is perpendicular to the face of the baffle where the loudspeaker is mounted (Fig. 4), hence the term, distributed edge dipole model.

It is known that the Kirchhoff approximation has been validated close to the forward direction only. Nevertheless for the DED model it will be assumed valid for all angles in order to show how the driving pressure changes continuously from the illuminated zone across the boundary to the shadow zone. This is fundamentally different from Vanderkooy's model since a continuous source avoids a discontinuity at the boundary. Limitations of the Kirchhoff

approximation and assumptions made in the formulation of the DED model are considered acceptable since we are primarily interested in modeling low-frequency diffraction effects at large observation distances.

Using finite-element analysis, Wright [4] confirmed that the edges are phase reversed in the illuminated zone and in phase in the shadow region. Wright also showed [4, fig. 2] that for a point source, along the shadow boundary ($\theta = 90°$), the sound pressure from the diffractive edges is zero and the pressure from the driving sound source is half of its forward value. This is in agreement with the DED model, that is, $K_{\text{DED}}(90°) = \frac{1}{2}$ and $F_{\text{DED}}(90°) = 0$.

It should be noted that as the frequency increases and the sound source is no longer a point source, the driving pressure on the edges will be less than half its forward value due to the increasing directivity of the source with frequency. (This will be discussed further in Section 2.2.)

1.4 Summary of the Three Models

Angular form factors for the driving force K and the edge pressure F for all three diffraction models are compared in Table 1 for the case of a thin circular baffle.

It should be noted that there are significant differences concerning the angular behavior of the driving pressure $K(\theta)$. For the DED model, $K(\theta)$ is continuous across the
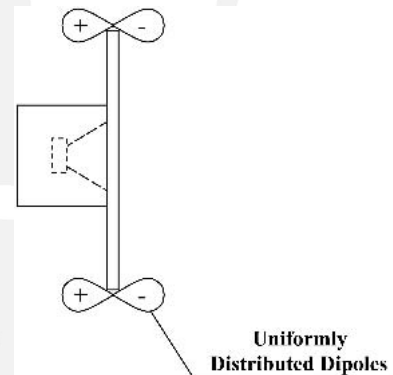

Fig. 4. DED model considers infinitely small dipoles distributed continuously along baffle edge (in this case along circumference of a thin circular baffle) and operating in phase opposition to driving source.

Table 1. Comparison of angular form factors for driving force K and edge pressure F for a thin circular baffle ($\theta_W = 0°$).

Model	$K(\theta)$	$K\left(\theta = \dfrac{\pi}{2}\right) F(\theta)$
Bews and Hawksford	1 when $\theta \leq 90°$ Not specified for $\pi > 90°$	$-\dfrac{1}{2}$
Vanderkooy	1 when $\theta \leq 90°$ θ when $\theta > 90°$	$-\dfrac{1}{2\cos(\chi/2)}$
DED model	$\dfrac{1 + \cos\theta}{2}$	$-\dfrac{1}{2}\cos\theta$

boundary whereas the Vanderkooy model postulates a discontinuous behavior.

The angular form factor for the elementary diffractive sources on the edges, $K(90°)F(\theta)$, is almost identical for the three models in the forward direction ($\theta = 0°$) in both amplitude and phase. The phase inversion is commonly predicted by all three models.

Significant differences are observed in other directions, especially at $\theta = 90°$, where the DED model predicts no contribution due to the edges whereas the Vanderkooy model predicts large values.

In the rear direction ($\theta > 90°$) the DED and Vanderkooy models change sign, the B&H model does not.

2 PREDICTIONS OF DED MODEL

2.1 Point Source in a Finite Circular Baffle

To further illustrate the effects of edge dipoles, we now consider a point source located at the center of a circular baffle with radius L,

$$P_{\text{drive}}(r, \theta) = \frac{1 + \cos \theta}{2} P_{\infty\text{baffle}}(r, \theta). \tag{12}$$

The pressure of a point source on an infinite baffle is

$$P_{\infty\text{baffle}}(r, \theta) = P_{\infty\text{baffle}}(r) = j\rho ckQ \frac{e^{-jkr}}{2\pi r} \tag{13}$$

where

ρ density of air, $= 1.2 \text{ kg/m}^3$
c sound velocity, $= 340 \text{ m/s}$
k wave number, $= 2\pi/\lambda$
Q strength of point source, m^3/s.

In the Appendix we obtained an expression for the elementary edge sources [Eq. (58)] that is valid in the forward direction only. As stated previously, for the DED model it is assumed that this expression remains valid at all angles, and we now proceed with this hypothesis.

In a given direction θ the uniform distribution of edge dipoles for the circular baffle produces pressure $P_{\text{edge}}(r, \theta)$,

$$P_{\text{edge}}(r, \theta) = -\cos \theta \frac{1}{2} P_{\infty\text{baffle}}(L) \int_0^{2\pi L} \frac{e^{-jkr_P}}{2\pi r_P} \, dl \tag{14}$$

$$P_{\text{edge}}(r, \theta) = -\cos \theta \frac{1}{2} \left(j\rho ckQ \frac{e^{-jkL}}{2\pi L} \right) \int_0^{2\pi L} \frac{e^{-jkr_P}}{2\pi r_P} \, dl \tag{15}$$

$$r_P = r - L \tag{16}$$

$$r_P^2 = r^2 + L^2 - 2r \cdot L. \tag{17}$$

For a distant observation point, $r \gg L$, therefore

$$r_P = r - \frac{r \cdot L}{r}. \tag{18}$$

We choose to rotate the x and y axes in the plane of the baffle so that r remains in the yz plane. Therefore, we have

$$r_P = r - L \sin \theta \sin \phi \tag{19}$$

$P_{\text{edge}}(r, \theta)$

$$= -\cos \theta \frac{1}{2} \left(j\rho ckQ \frac{e^{-jkL}}{2\pi L} \right) \int_0^{2\pi L} \frac{e^{-jkr} e^{jkL \sin \theta \sin \phi}}{2\pi r} \, dl$$

$$= -\cos \theta \frac{1}{2} \left(j\rho ckQ \frac{e^{-jkr}}{2\pi r} \right) \int_0^{2\pi L} \frac{e^{-jkL} e^{jkL \sin \theta \sin \phi}}{2\pi L} \, dl$$

$$= -\frac{P_{\infty\text{baffle}}(r)}{2} \cos \theta \, e^{-jkL} \frac{1}{2\pi} \int_0^{2\pi} e^{jkL \sin \theta \sin \phi} \, d\theta$$

$$= -P_{\infty\text{baffle}}(r) \frac{\cos \theta}{2} e^{-jkL} J_0(kL \sin \theta) \tag{20}$$

and the total pressure in direction θ will be

$$P_{\text{total}}(r, \theta) = P_{\text{drive}}(r, \theta) + P_{\text{edge}}(r, \theta)$$

$$= P_{\infty\text{baffle}}(r) \frac{1 + \cos \theta}{2}$$

$$- P_{\infty\text{baffle}}(r) \frac{\cos \theta}{2} e^{-jkL} J_0(kL \sin \theta)$$

$$\frac{P_{\text{total}}(r, \theta)}{P_{\infty\text{baffle}}(r)} = \frac{1 + \cos \theta}{2} - \frac{\cos \theta}{2} e^{-jkL} J_0(kL \sin \theta). \tag{21}$$

It should be noted that for $\theta = 0$ (the forward direction), the Bessel function $J_0 = 1$ and Eq. (21) then reduces to the result obtained in the Appendix [Eq. (53)].

At low frequencies, where $kL < 1$ or f (Hz) $< 50/L$ (m), we can approximate the exponential and the Bessel function by 1,

$$\frac{P_{\text{total}}(r, \theta)}{P_{\infty\text{baffle}}(r)} = \left(\frac{1 + \cos \theta}{2} - \frac{\cos \theta}{2} \right) = \frac{1}{2}. \tag{22}$$

We thus have an isotropic angular distribution for the pressure, and the amplitude is half the value of the pressure for the same point source when mounted on an infinite baffle.

The total pressure on axis for a point source in a finite circular baffle can therefore be expressed as

$$P_{\text{total}}(r, 0°) = P_{\infty\text{baffle}}(r) \left[\frac{1 + \cos(0°)}{2} - \frac{\cos(0°)}{2} e^{-jkL} \right]. \tag{23}$$

The forward SPL is given by

$$\text{forward SPL} = 10 \log_{10} |P_{\text{total}}|^2 + \text{constant}$$

$$= 10 \log_{10} \left\{ |P_{\infty\text{baffle}}|^2 \left(\left[1 - \frac{\cos(kL)}{2} \right]^2 \right. \right.$$

$$\left. \left. + \left[\frac{\sin(kL)}{2} \right]^2 \right) \right\} + \text{constant}. \qquad (24)$$

Normalizing by the infinite baffle SPL gives

$$\text{forward SPL (baffle of radius } L) - \text{forward SPL } (\infty\text{baffle})$$

$$= 10 \log_{10} \left[1 + \frac{1}{4} - \cos(kL) \right]. \qquad (25)$$

Referring to Fig. 5, the DED model predicts that the SPL in the forward direction oscillates from −6 to +3.5 dB. For $L = 0.4$ m the first maximum will occur at 425 Hz, in agreement with the result presented by Beranek in 1954 [5, p. 238]. It is verified that the low-frequency SPL for a point source under circular baffle mounting conditions is 6 dB below the SPL for the infinite baffle case.

2.2 Extended Source in a Finite Circular Baffle

Compared to the point source case, for an extended sound source of radius R, the Bessel function is used to characterize $P_{\infty\text{baffle}} (r, \theta)$,

$$P_{\infty\text{baffle}}(r, \theta) = j\rho ckQ \frac{2J_1(kR \sin \theta)}{kR \sin \theta} \frac{e^{-jkr}}{2\pi r}. \qquad (26)$$

The driving pressure is

$$P_{\text{drive}}(r, \theta) = \frac{1 + \cos \theta}{2} P_{\infty\text{baffle}}(r, \theta). \qquad (27)$$

When $\theta = 90°$ this reduces to

$$P_{\text{drive}}(r = L, 90°) = \frac{1}{2} j\rho ckQ \frac{2J_1(kR)}{kR} \frac{e^{-jkL}}{2\pi L}. \qquad (28)$$

The driving pressure is inversely proportional to the frequency. In other words, the strength of the edge dipoles will be reduced at higher frequencies. This is expected since the driving sound source is becoming more directive as the frequency increases and does not energize the edges as much. Fig. 6 displays the SPL versus frequency of a 12-in (0.3-m) loudspeaker mounted on a 0.5-m-radius circular baffle.

3 EXPERIMENTAL DATA

It was necessary to perform polar measurements of the absolute SPL of a test loudspeaker mounted on an infinite baffle in order to compare with measurements of the same loudspeaker mounted on a finite circular baffle. This allows for the extraction of the characteristic departures of finite baffle mounting from infinite baffle behavior. The infinite baffle is approximated by the ground and the loudspeaker test configuration is pictured in Fig. 7.

3.1 Description of Experimental Setup

Measurements were performed outdoors to improve low-frequency resolution. A 12-in (0.3-m) loudspeaker component was selected in order to provide sufficient SPL output at 50 Hz while at the same time allowing for the measurement of edge dipole effects up to 1 kHz. The loudspeaker component was mounted in a cylindrical cabinet filled with damping material, forming a 46-L-volume sealed enclosure. A 24-dB/oct high-pass filter was inserted at 30 Hz with a 10-dB boost at 50 Hz in the signal chain in order to obtain an on-axis frequency response as flat as possible in the low-frequency range. Applying a 12-V rms pink-noise signal to the loudspeaker yielded a satisfactory measured SPL that was 20 dB above the ambient noise centered at 50 Hz without reaching the loudspeaker's maximum excursion. In addition, a pink-noise weighted maximum-length-sequence (MLS) signal provided low-frequency preemphasis and improved the signal-to-noise
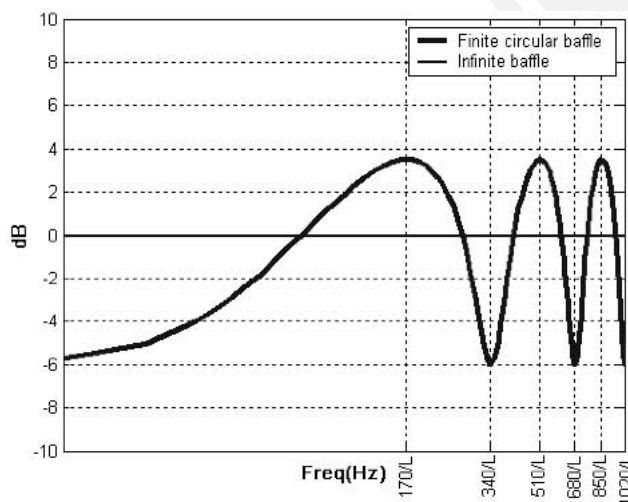

Fig. 5. Forward SPL normalized at 1 m for a point source mounted on a circular baffle of radius L (meters) compared with a point source mounted in an infinite baffle for a distant observation point.
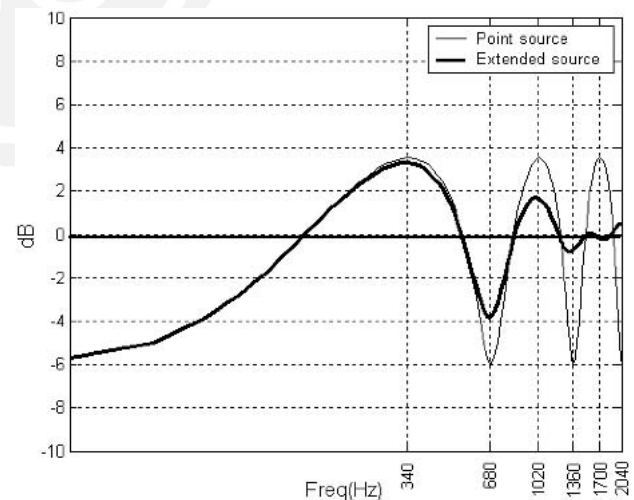

Fig. 6. Comparison between forward SPL normalized at 1 m for a point source and an extended source in a closed cabinet with a circular and thin baffle of radius $L = 0.5$ m for a distant observation point. $R = 0.128$ m = effective radius of 12-in (0.3-m) loudspeaker component used experimentally.

ratio in the bass region significantly. The frequency response was then calculated using the fast Fourier transform of the impulse response obtained by the cross-correlation operation between the MLS signals that are generated and measured by the analyzer. The frequency response obtained was then considered as a sensitivity measurement at 2.83 V rms at 1 m for a system with 8 Ω nominal impedance. The frequency resolution and the step between any two frequencies were equal to 50 Hz.

3.2 Infinite Baffle

For the test setup pictured in Fig. 7 the observation point was 2.16 m away, and measurements were taken from on axis (0°) to 90° in 10 steps. The SPL is shown in Fig. 8 as

a function of frequency, and it can be seen that the sound source has isotropic behaviour up to 300 Hz while behaving as a point source at lower frequencies.

3.3 Thin Circular Baffle

A second series of measurements was carried out in order to determine the loudspeaker behavior in a finite baffle. A circular wooden baffle with 0.5-m radius and a thickness of 40 mm (wedge angle = 0) was constructed, and the same 12-in (0.3-m) test loudspeaker was mounted in this baffle. A test fixture was constructed to suspend the cabinet and its circular baffle plus the microphone at a height of 4.15 m (Fig. 9). The observation point was 2.16 m away, and the SPL was measured from 0 to 180° in
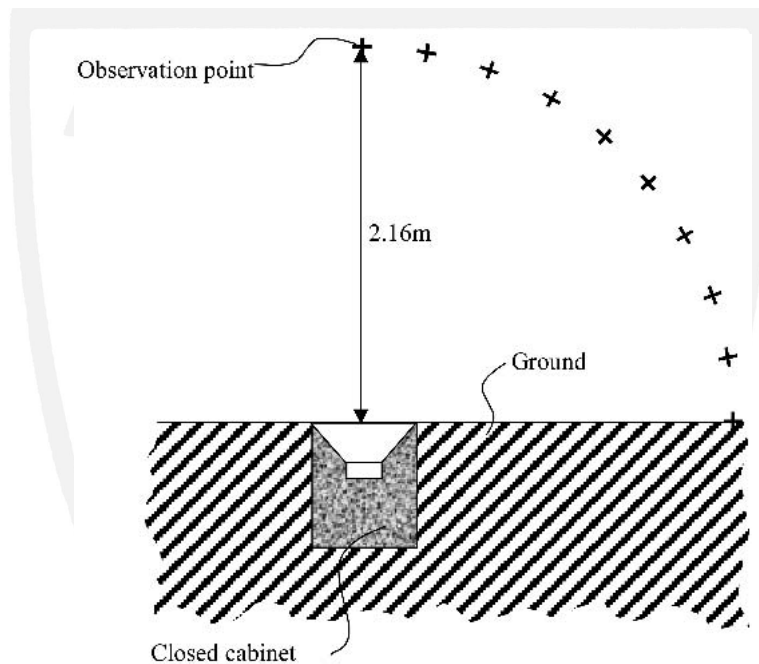

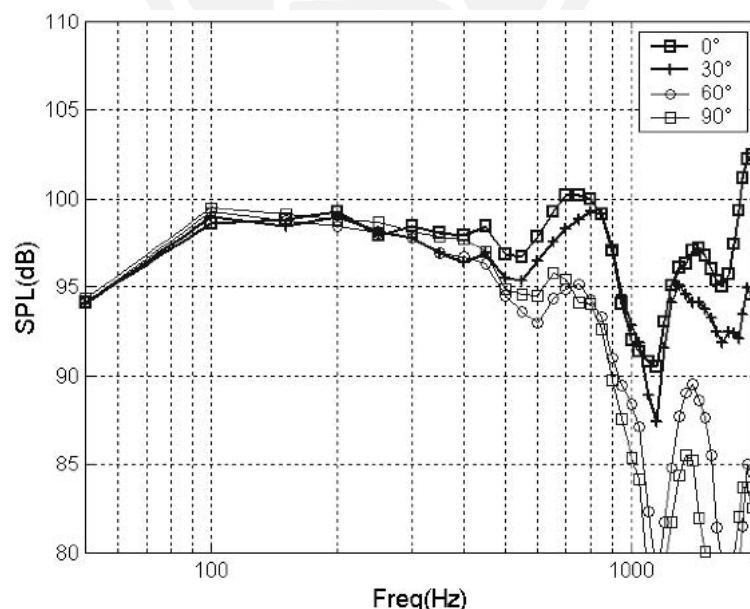Fig. 7. Experimental setup for infinite baffle measurements.

Fig. 8. Frequency responses at θ = 0°, 30°, 60°, 90° for 12-in (0.3-m) loudspeaker mounted in an infinite baffle (2.16-m measurement distance).

steps of 5° in the horizontal plane (Fig. 10) at a frequency resolution of 50 Hz.

The SPL versus angle for infinite and finite baffles is shown in Figs. 11–15 at five different frequencies. Note that the infinite baffle has an angular range that stops at 90°. At 50 Hz (Fig. 11) it is seen that the forward SPL for the infinite-baffle case is 4 dB above the finite-baffle configuration. The finite-baffle case shows some directivity, and it is interesting to note the 4-dB loss between the forward and backward regions since the radius of the baffle is 14 times smaller than the wavelength. As expected, the SPL for the infinite-baffle configuration remains constant with angle at 50 Hz.

As predicted in Fig. 6, the forward SPL of the infinite baffle will be equal to the forward SPL of the finite baffle

at 150 Hz. This is verified by the measurements shown in Fig. 12. It is also seen that at 150 Hz the finite baffle becomes more directive while the infinite-baffle SPL still remains constant with the angle. As predicted in Fig. 6, the first SPL maximum will occur around 340 Hz.

Experimental results at 300 Hz, shown in Fig. 13, indicate that the finite baffle delivers more power in the forward direction than the infinite baffle. While the infinite baffle is still constant with the angle, the SPL of the finite baffle shows a pronounced notch at θ = 125°. The first forward SPL minimum should occur at 680 Hz. The experimental results of Fig. 14, performed at 650 Hz, confirm this, and it is interesting to note that the SPL for the finite-baffle case is maximum at an angle of 35° with a pronounced notch at θ = 150°. It is also seen
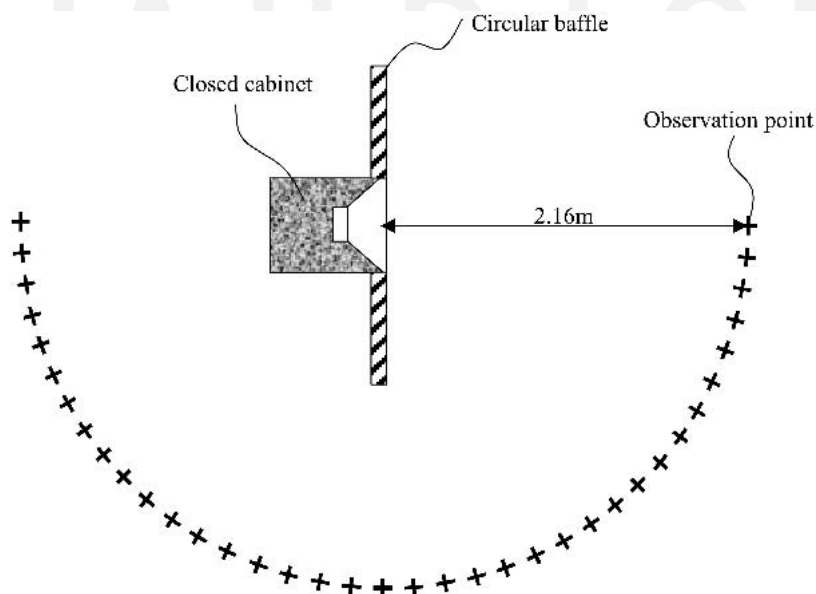

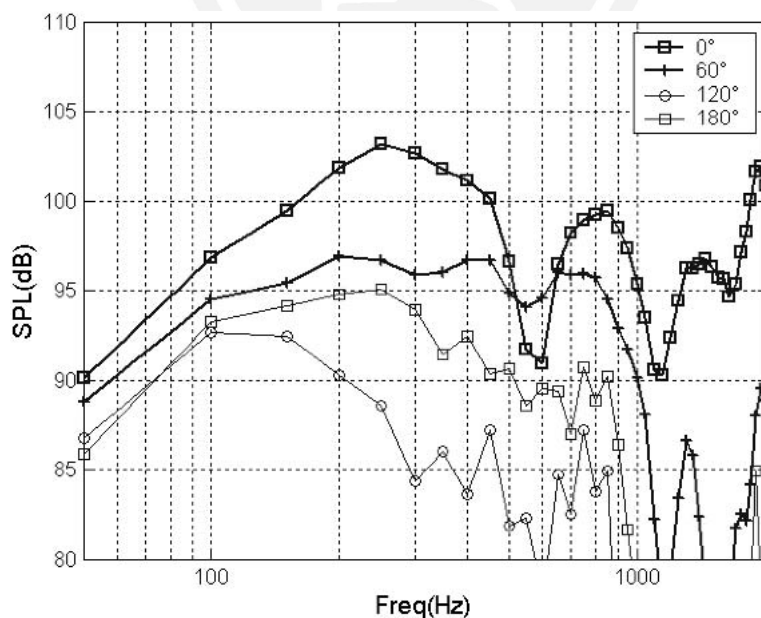Fig. 9. Experimental setup for measurements in finite circular baffle (top view).

Fig. 10. Frequency responses at θ = 0°, 60°, 120°, 180° for 12-in (0.3-m) loudspeaker mounted in a finite thin circular baffle (2.16-m measurement distance).
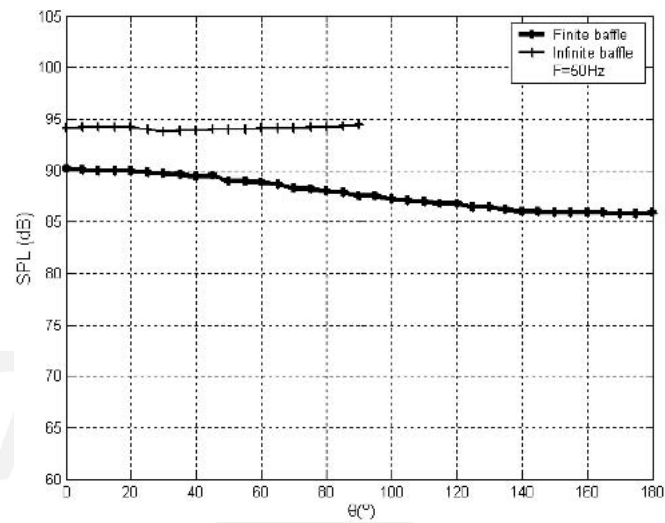
Fig. 11. SPL as a function of angle at $F = 50$ Hz for thin circular baffle.
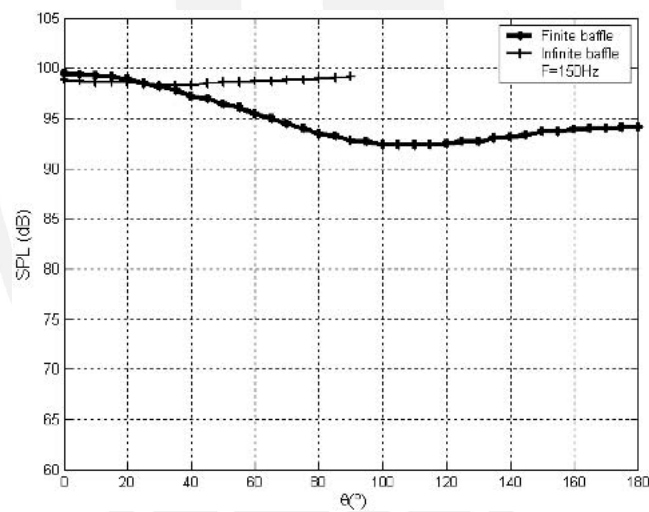

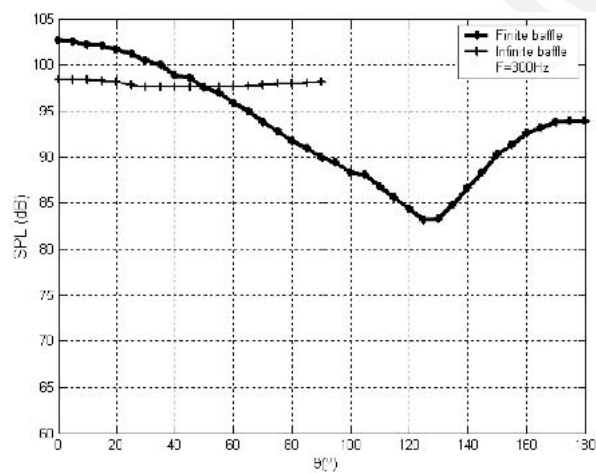Fig. 12. SPL as a function of angle at $F = 150$ Hz for thin circular baffle.

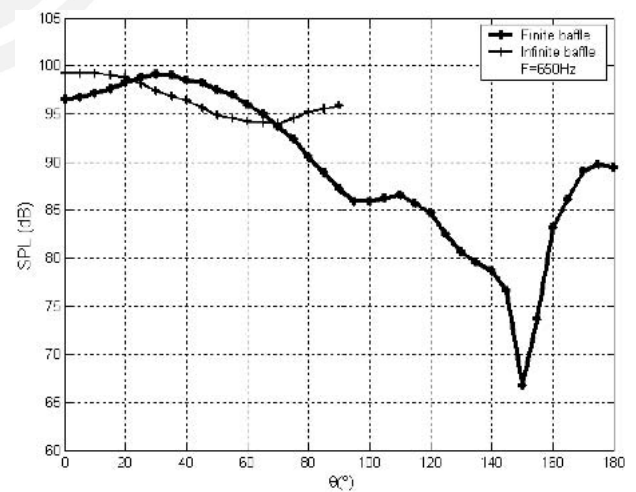Fig. 13. SPL as a function of angle at $F = 300$ Hz for thin circular baffle.

Fig. 14. SPL as a function of angle at $F = 650$ Hz for thin circular baffle.

that the infinite-baffle configuration starts to become directive.

In the experimental results of Fig. 15 the infinite baffle shows a higher degree of directivity while the SPL for the finite baffle exhibits two pronounced notches at $\theta = 120°$ and $160°$.

4 COMPARISON OF MODELS WITH EXPERIMENTAL DATA FOR A THIN CIRCULAR BAFFLE

To simplify the comparison between all three models, the measured frequency response of the 12-in (0.3-m) loudspeaker mounted in the infinite baffle is used as a reference for normalizing the experimental data. To perform the normalization operation, the forward SPL as measured under infinite-baffle mounting conditions is subtracted from all angular measurements for finite-baffle mounting conditions.

The comparison of the models is carried out using the following formulas:

- *B&H Model [2]* Since the value of P_{drive} in the shadow region is not specified in [2], B&H modeling results are presented for $\theta = 0°$ to $90°$ only,

$$
P_{total}(r, \theta)
$$

$$
= P_{\infty baffle}(r, \theta) - \frac{1}{2} P_{\infty baffle}(r = L, \theta = 90°) \int_0^{2\pi L} \frac{e^{-jkr_P}}{2\pi r_P} \, dl. \tag{29}
$$

- *Vanderkooy Model [3]*
  For $\theta < 90°$ (illuminated zone),

$$
P_{total}(r, \theta) = P_{\infty baffle}(r, \theta) - P_{\infty baffle}(r = L, \theta = 90°)
$$

$$
\times \int_0^{2\pi L} \frac{1}{2 \cos(\chi/2)} \frac{e^{-jkr_P}}{2\pi r_P} \, dl. \tag{30}
$$

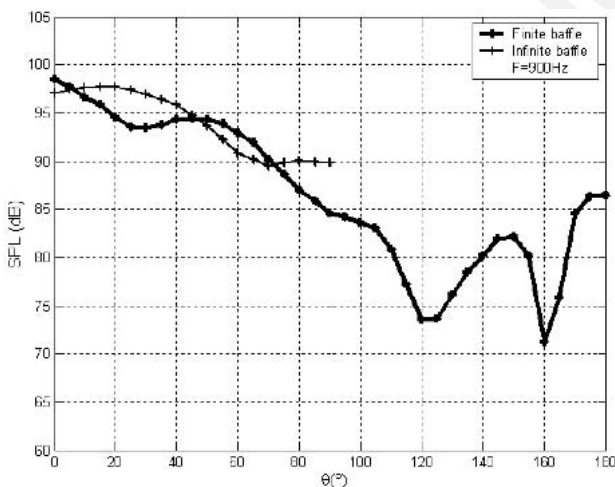
Fig. 15. SPL as a function of angle at $F = 900$ Hz for thin circular baffle.

For $\theta > 90°$ (shadow zone), $P_{drive} = 0$ in the shadow zone. Therefore

$$
P_{total}(r, \theta)
$$

$$
= 0 - P_{\infty baffle}(r = L, \theta = 90°) \int_0^{2\pi L} \frac{1}{2 \cos(\chi/2)} \frac{e^{-jkr_P}}{2\pi r_P} \, dl. \tag{31}
$$

- *DED Model* For the DED model, P_{drive} is continuous from the illuminated zone to the shadow zone,

$$
P_{total}(r, \theta) = \frac{1 + \cos\theta}{2} P_{\infty baffle}(r, \theta)
$$

$$
- \frac{\cos\theta}{2} P_{\infty baffle}(r = L, \theta = 90°) \int_0^{2\pi L} \frac{e^{-jkr_P}}{2\pi r_P} \, dl. \tag{32}
$$

For all models,

$$
P_{\infty baffle}(r, \theta) = j\rho ckQ \frac{2J_1(kR \sin\theta)}{kR \sin\theta} \frac{e^{-jkr}}{2\pi r} \tag{33}
$$

where $r = 2.16$ m, $L = 0.5$ m, and $R = 0.128$ m.

Results are normalized by dividing by the infinite-baffle pressure,

$$
P_{\infty baffle}(r, \theta = 0°) = j\rho ckQ \frac{2J_1(kR \sin 0°)}{kR \sin 0°} \frac{e^{-jkr}}{2\pi r} = j\rho ckQ \frac{e^{-jkr}}{2\pi r}. \tag{34}
$$

Let us first consider the forward SPL. Subtracting the SPL of Fig. 8 from the SPL of Fig. 10 gives the results shown in Fig. 16. Fig. 16 can be compared directly with Fig. 6. In Fig. 16 it is to be noted that all three models are in close agreement in the forward direction.

However, as seen in Figs. 17–21, significant differences occur between models off axis. In these figures the SPL for the finite-baffle case is normalized by the forward SPL of the infinite baffle and then plotted as a function of angle for the discrete frequencies considered in Section 3.3.

In Figs. 17–21 it is seen that the B&H model does not exhibit high enough directivity. For frequencies above 150 Hz the Vanderkooy model reproduces very well the forward and backward measurements, but predictions around $\theta = 90°$ are divergent. The DED model offers a better consistency over the whole angular and frequency ranges.

5 COMPARISON OF MODELS WITH EXPERIMENTAL DATA FOR A RECTANGULAR LOUDSPEAKER ENCLOSURE

We now present measurements and simulation results for the rectangular loudspeaker enclosure depicted in Fig. 22. Ground-plane measurements were performed outdoors with the microphone at a 3.16-m distance from the center of the front face of the enclosure. The measurements were taken from on axis to $180°$ in $10°$ steps, around the *ZOZ'* axis as shown in Fig. 22.

As depicted in Fig. 23, the edges of the front baffle and of its ground-plane image are the location of the elemen-
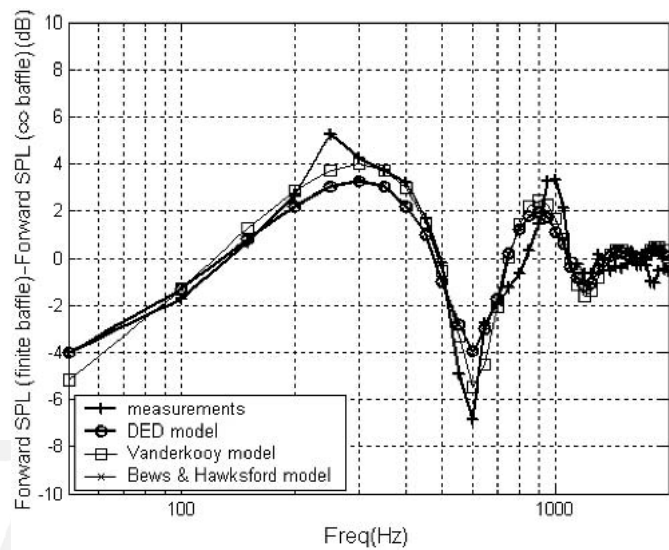
Fig. 16. Normalized on-axis frequency response, measurements versus model predictions.
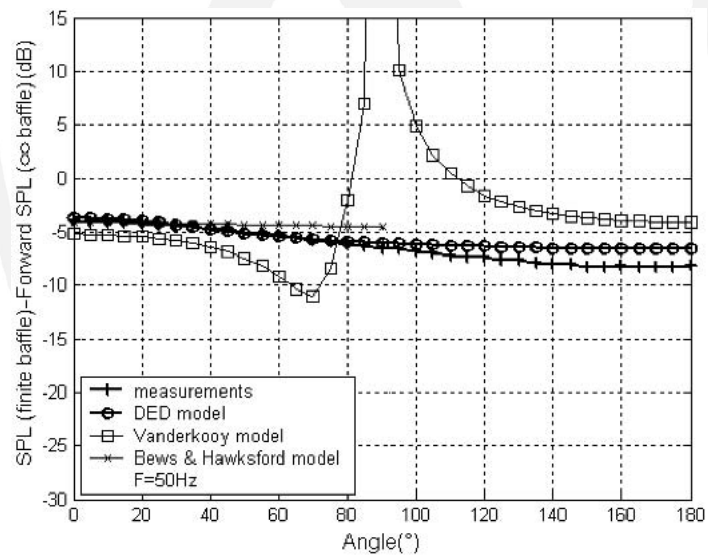

Fig. 17. Normalized SPL as a function of angle at $F = 50$ Hz for thin circular baffle.

Fig. 18. Normalized SPL as a function of angle for $F = 150$ Hz for thin circular baffle.

Fig. 19. Normalized SPL as a function of angle for $F = 300$ Hz for thin circular baffle.
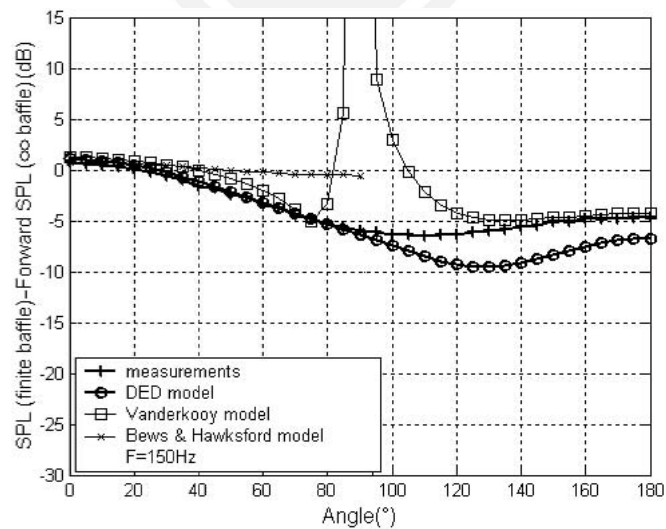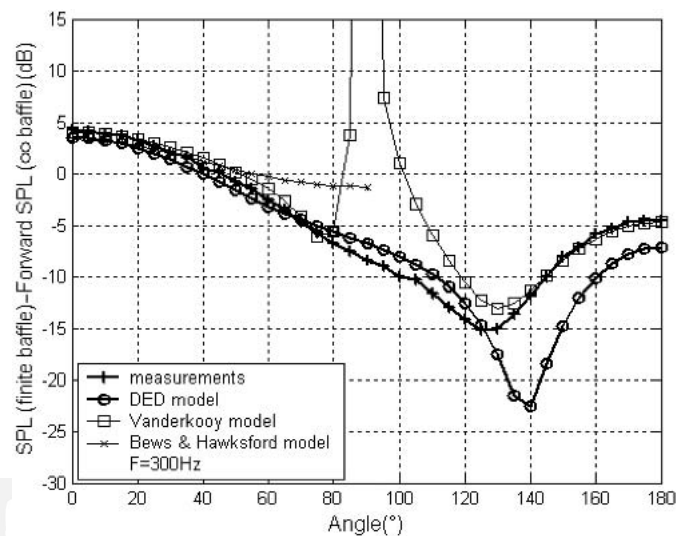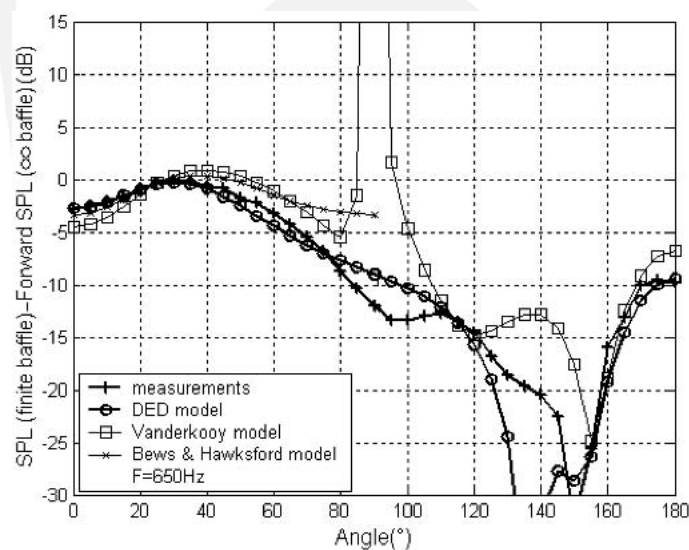

Fig. 20. Normalized SPL as a function of angle for $F = 650$ Hz for thin circular baffle.
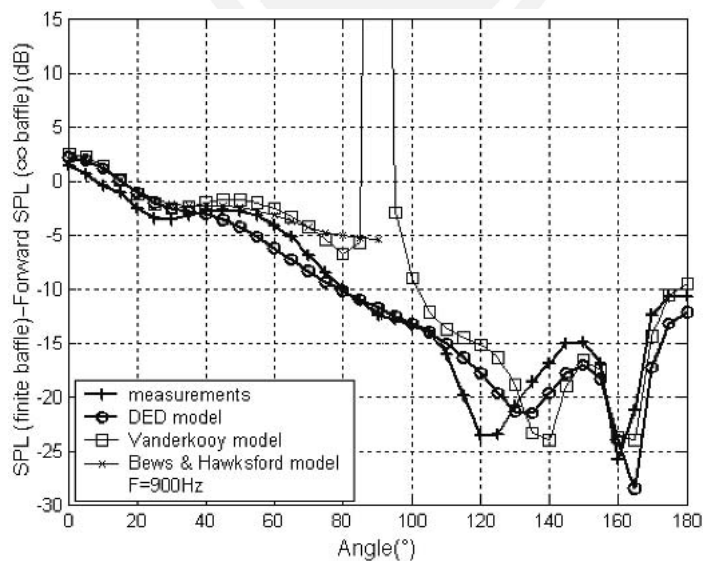

Fig. 21. Normalized SPL as a function of angle for $F = 900$ Hz for thin circular baffle.

tary diffraction edge sources (represented as small full circles in the middle of each elementary segment). For modeling purposes, the spacing between elementary sources is chosen to be much smaller than the wavelength associated with the highest frequency of interest (300 Hz). Measurements of SPL as a function of angle are compared with the three model predictions at 150 and 300 Hz (Figs. 24 and 25, respectively).

For a rectangular enclosure the wedge angle $\theta_W = 90°$. Therefore, from Eqs. (5) and (6) we obtain the correspond-

Fig. 22. Dimensions (meters) of thick rectangular baffle and mounting position of loudspeaker component.

(a)

The axes of the dipoles are perpendicular to the front baffle plane

(b)

Fig. 23. Edges of baffle and their image on the ground have been replaced by densely spaced elementary edge sources (small full circles). (a) Front view. (b) Top view, showing that dipole axes for the DED model are perpendicular to front baffle plane.

ing edge source terms for the B&H and Vanderkooy models,

$$F_{\mathrm{BH}} = -\frac{1}{3}, \qquad F_{\mathrm{V}}(\chi) = -\frac{2}{\sqrt{3}}\frac{1}{1 + 2\cos(2\chi/3)}.$$

Contrary to these two models, the DED model makes the assumption that the dipole edge sources do not depend on the wedge angle. The axes of the dipoles in the DED model are thus kept perpendicular to the front baffle plane, as shown in Fig. 23, and as a first approximation we use the same form factor as for the thin-baffle case,

$$F_{\mathrm{DED}}(\theta) = -\cos\theta.$$

The question arises as to what is the relative weighting of the elementary edge sources for the three models. The driving pressure propagates to the baffle edges and distributes itself equally in ϕ, the polar angle of the baffle plane (Fig. 3). The relative weight of each elementary edge source is thus given for the three models by the ratio of the angle subtended by the elementary segment from the driving sound source with 2π. For instance, the driving source S_1 excites the elementary edge source n with a weight $d\alpha_{1n}/(2\pi)$ and the image driving source S_2 excites the same edge source n with a smaller weight, $d\alpha_{2n}/(2\pi)$.

It can be seen in Figs. 24 and 25 that the B&H model is still not directive enough and the Vanderkooy model is too large around 90° and too high in the backward region. The DED model is seen to reproduce the measurements well at all angles and for both frequencies.

6 CONCLUSIONS

A new model that takes into account the diffraction effects produced by cabinet edges on the SPL radiated by a loudspeaker has been presented. The model is termed the distributed edge dipole (DED) model since it represents secondary edge diffraction effects using a uniform distribution of dipoles whose axes are perpendicular to the front baffle plane.

The DED model was compared to two previous modeling techniques, and all three models were compared with measurements. Measurements were performed first on a thin circular baffle to emphasize edge diffraction effects and allow for comparison between all three models versus measurements from 50 to 1000 Hz and from 0 to 180°. A second set of measurements was carried out on a rectangular loudspeaker enclosure at two frequencies as a function of the angle.

For both test cases, good agreement was observed between measurements and DED model predictions, indicating that the DED model allows for improved, more accurate modeling of loudspeaker SPL versus angle and frequency. In particular, significant improvements are obtained in the boundary region between the forward and backward directions using the DED model.

7 ACKNOWLEDGMENT
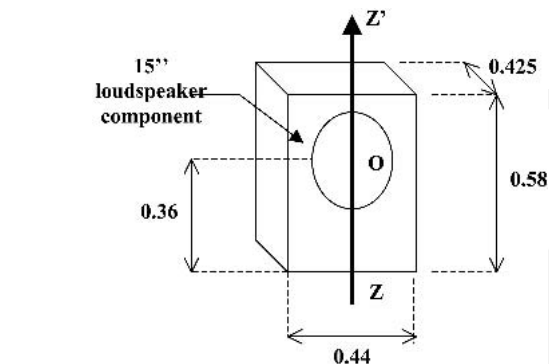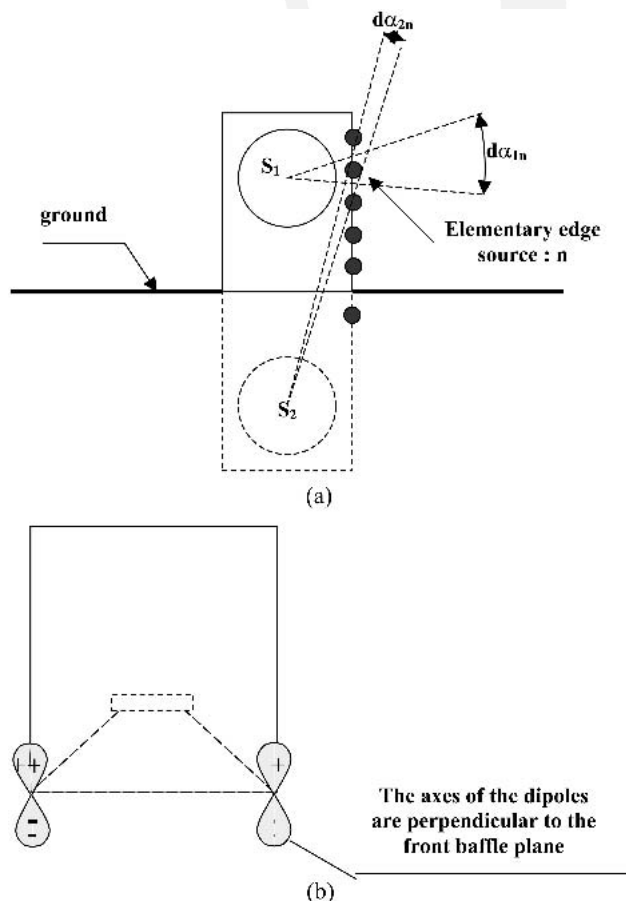
8 REFERENCES

[1] H. F. Olson, *Acoustical Engineering* (Van Nostrand, Princeton, NJ, 1957), pp. 17–19.

[2] R. M. Bews and M. J. Hawksford, *J. Audio Eng. Soc.,* "Application of the Geometric Theory of Diffraction (GTD) to Diffraction at the Edges of Loudspeaker Baffles," vol 34, pp. 771–779 (1986 Oct.).

[3] J. Vanderkooy, *J. Audio Eng. Soc.,* "A Simple Theory of Cabinet Edge Diffraction," vol 39, pp. 923–933 (1991 Dec.).

[4] J. R. Wright, *J. Audio Eng. Soc.,* "Fundamentals of Diffraction," vol 45, pp. 347–356 (1997 May).

[5] L. L. Beranek, *Acoustics,* 3rd printing (American Institute of Physics, New York, 1990).

[6] P. K. Banerjee and R. Butterfield, *Boundary Element Methods in Engineering Science* (McGraw-Hill, New York, 1981).

[7] G. M. Jebsen and H. Medwin, *J. Acoust. Soc. Am.,* vol. 72, pp. 1607–1611 (1982).

APPENDIX
MATHEMATICAL DERIVATION OF DED MODEL

We first recall the Helmholtz–Kirchhoff integral solution for the sound field produced by an enclosed piston in a baffle. Second, the Kirchhoff approximation is made and the resultant sound field is formulated as a dipolar form of the edge diffraction which is the basis for the DED model.
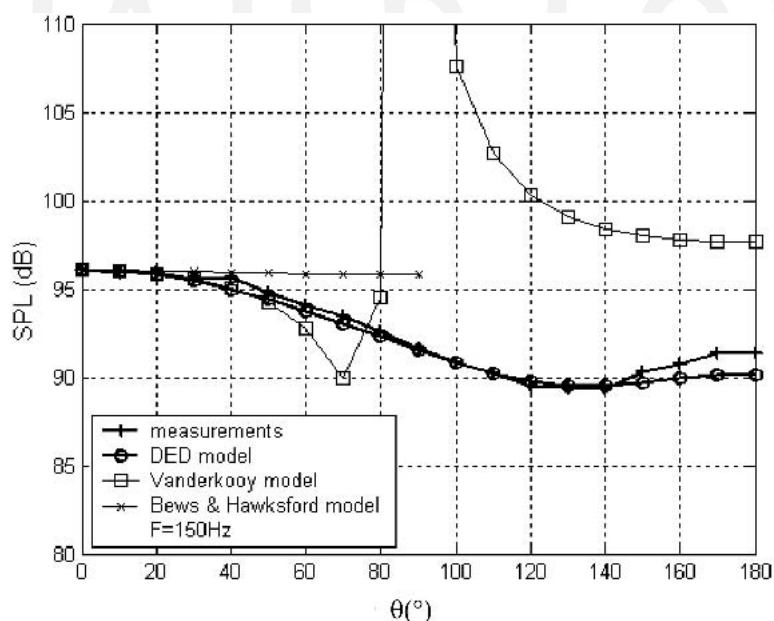

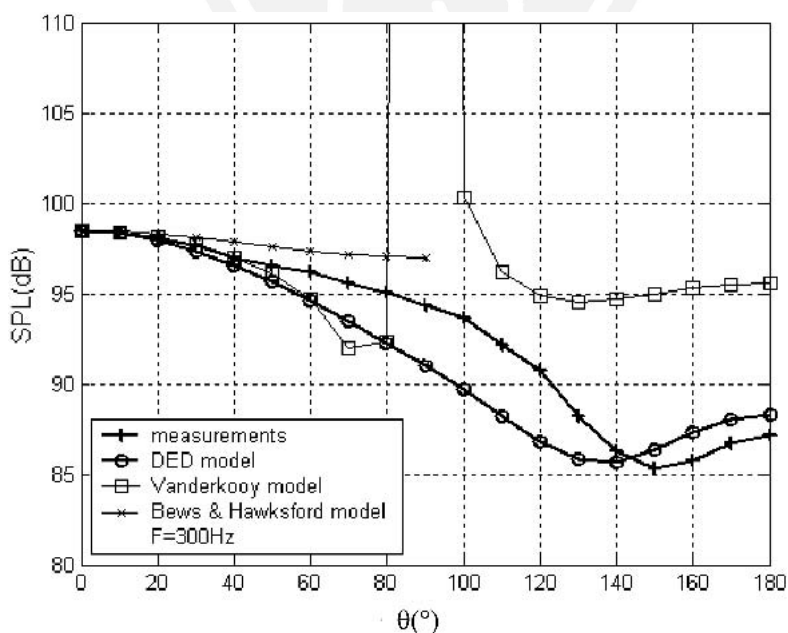Fig. 24. SPL as a function of angle at F = 150 Hz for thick rectangular baffle.

Fig. 25. SPL as a function of angle at F = 300 Hz for thick rectangular baffle.

Defining p as the acoustic pressure, only periodic solutions are considered and therefore the time dependence factors out,

$$p(\boldsymbol{r},\ t) = p(\boldsymbol{r})e^{j\omega t} . \tag{35}$$

With reference to Fig. 1 we define a closed surface S consisting of a piston, a thin circular baffle, and an enclosure. From Green's second identity,

$$\iiint_V (p\Delta G - G\Delta p)\,dV = \iint_S \left(p\frac{\partial G}{\partial n} - G\frac{\partial p}{\partial n}\right)dS \tag{36}$$

where V is the exterior volume defined by surface S and n is the normal to the surface S, directed outward.

A point running on the surface S is denoted by the vector $\boldsymbol{r}_1$, and the point of observation is denoted by the vector $\boldsymbol{r}_2$.

Defining G as the Green's function,

$$G(\boldsymbol{r}_1, \boldsymbol{r}_2) = \frac{e^{-jk_{r12}}}{4\pi r_{12}} \tag{37}$$

where

$$r_{12} = |\boldsymbol{r}_2 - \boldsymbol{r}_1|.$$

The pressure will obey the Helmholtz equation,

$$\Delta p + k^2 p = 0 \tag{38}$$

and the Green's function will obey

$$\Delta G + k^2 G = -\delta(\boldsymbol{r}_{12}). \tag{39}$$

Transforming the Helmholtz equation using the integral method [6],

$$\iiint_V [-p\delta(\boldsymbol{r}) - k^2 pG + k^2 pG]\,dV = \iint_S \left(p\frac{\partial G}{\partial n} - G\frac{\partial p}{\partial n}\right)dS \tag{40}$$

and

$$p(\boldsymbol{r}_2) = -\iint_S \left(p\frac{\partial G}{\partial n} - G\frac{\partial p}{\partial n}\right)dS. \tag{41}$$

The normal derivative of the pressure and of the Green's function is

$$\frac{\partial p}{\partial n} = jk\rho c\,\frac{\boldsymbol{n}}{n}\cdot\boldsymbol{u} \tag{42}$$

$$\frac{\partial G}{\partial n} = \frac{\boldsymbol{n}}{n}\cdot\boldsymbol{\nabla}G = G\cos(\boldsymbol{n}, \boldsymbol{r}_{12})\left(-jk - \frac{1}{r_{12}}\right) \tag{43}$$

where u is the velocity on the surface S.

We then have the pressure at point $\boldsymbol{r}_2$, external to S, as an integral over the point $\boldsymbol{r}_1$ running on the surface S,

$$p(\boldsymbol{r}_2) = \int_S \left\{p(\boldsymbol{r}_1)G\cos(\boldsymbol{n}, \boldsymbol{r}_{12})\left(jk + \frac{1}{r_{12}}\right)\right.$$

$$\left. + G\,jk\rho c\left[\boldsymbol{u}(\boldsymbol{r}_1)\cdot\frac{\boldsymbol{n}}{n}\right]\right\}d\boldsymbol{r}_1. \tag{44}$$

In order to evaluate this integral the pressure and the normal velocity on the surface S are needed. The normal velocity is zero everywhere on the surface S, except for the surface of the piston. Thus we only require the value of the pressure on S.

A.1 Kirchhoff Approximation to Obtain Pressure on Surface S

When the observation point is on the surface S, there is a discontinuity from the normal derivative of the Green's function and the integral gives only half the pressure. By imposing r_1 and r_2 as restricted to S,

$$\frac{p(\boldsymbol{r}_2)}{2} = \int_S \left[p(\boldsymbol{r}_1)\,G\cos(\boldsymbol{n}, \boldsymbol{r}_{12})\left(jk + \frac{1}{r_{12}}\right)\right.$$

$$\left. + jk\rho c\,\boldsymbol{u}(\boldsymbol{r}_1)\cdot\frac{\boldsymbol{n}}{n}\,G\right]d\boldsymbol{r}_1. \tag{45}$$

We will assume that the pressure is significant only on the front baffle surface and therefore n is normal to r_{12}. This is the Kirchhoff assumption, which has been shown to be valid essentially in the forward direction [7]. The first term in the integral is then equal to zero. As stated previously, the normal component of the velocity is zero, except on the source. Thus the only term in the integral is over the source,

$$p(\boldsymbol{r}_2) = 2jk\rho cQ\,\frac{e^{-jkr_{12}}}{4\pi r_{12}} \tag{46}$$

where

$$Q = \int_{\text{source}} u\,dS. \tag{46}$$

For our approximation the pressure on the front baffle surface is thus given by the pressure produced by the point source in an infinite baffle.

A.2 Estimation of Pressure Far away from Sound Source

We now return to the expression for the pressure at a distant observation point in the direction θ not too far from the forward direction. In this case the $1/r$ factor in front of jk can be neglected ($kr \gg 1$) and the Green's function can be considered independent of r_1 and equal to

$$G(\boldsymbol{r}_1, \boldsymbol{r}_2) = G(r_2) = \frac{e^{-jkr_2}}{4\pi r_2}. \tag{47}$$

Placing the sound source at the origin, r_1 is the distance from the source to a point on the front surface and r_2 is the distance from the origin to the point of observation.

Let us define

$$\cos\theta = \cos(\boldsymbol{n}, \boldsymbol{r}_{12}). \tag{48}$$

Then

$$p(\boldsymbol{r}_2) = \int_{\text{front surface}} \left(jk\rho cQ\,\frac{e^{-jkr_1}}{2\pi r_1}\,jkG\cos\theta\right.$$

$$\left. + jk\rho cuG\right)2\pi r_1\,dr_1. \tag{49}$$

The angle θ can be considered as constant for a distant observation point. Therefore,

$$p(\mathbf{r}_2) = \mathrm{j}k\rho cQ \cos\theta\, G(r_2) \int\limits_{\text{front surface}} \mathrm{e}^{-\mathrm{j}kr_1}\mathrm{j}k\,\mathrm{d}r_1$$

$$+ \mathrm{j}k\rho cQ\, G(r_2). \qquad (50)$$

The radius of the disk being L, the pressure can be written as

$$p(\mathbf{r}_2) = \frac{P_{\infty\text{baffle}}(r_2)}{2}\cos\theta\int\limits_0^L \mathrm{e}^{-\mathrm{j}kr_1}\,\mathrm{j}k\,\mathrm{d}r_1 + \frac{P_{\infty\text{baffle}}(r_2)}{2}. \qquad (51)$$

With

$$P_{\infty\text{baffle}}(r_2) = \mathrm{j}k\rho cQ\frac{\mathrm{e}^{-\mathrm{j}kr_2}}{2\pi r_2} \qquad (52)$$

then

$$p(\mathbf{r}_2) = P_{\infty\text{baffle}}(r_2)\frac{1+\cos\theta}{2} - P_{\infty\text{baffle}}(r_2)\frac{\cos\theta}{2}\mathrm{e}^{-\mathrm{j}kL}. \qquad (53)$$

We reformulate this expression,

$$p(\mathbf{r}_2) = P_{\text{drive}} + \int\limits_{\text{edge}}\frac{\mathrm{d}P_{\text{edge}}}{\mathrm{d}l}\,\mathrm{d}l. \qquad (54)$$

Inspection of Eqs. (52) and (53) gives

$$P_{\text{drive}}(r_2,\theta) = P_{\infty\text{baffle}}(r_2)\frac{1+\cos\theta}{2} \qquad (55)$$

and the edge effects as

$$\int\limits_{\text{edge}}\frac{\mathrm{d}P_{\text{edge}}}{\mathrm{d}l}\,\mathrm{d}l = -P_{\infty\text{baffle}}(r_2)\frac{\cos\theta}{2}\mathrm{e}^{-\mathrm{j}kL}$$

$$= -\mathrm{j}\rho ckQ\frac{\mathrm{e}^{-\mathrm{j}kr_2}}{2\pi r_2}\frac{\cos\theta}{2}\mathrm{e}^{-\mathrm{j}kL}. \qquad (56)$$

We can rearrange terms,

$$\int\limits_{\text{edge}}\frac{\mathrm{d}P_{\text{edge}}}{\mathrm{d}l}\,\mathrm{d}l = -\cos\theta\;\mathrm{j}\rho ckQ\frac{\mathrm{e}^{-\mathrm{j}kL}}{2\pi L}\frac{1}{2}2\pi L\frac{\mathrm{e}^{-\mathrm{j}kr_2}}{2\pi r_2}$$

$$= -\cos\theta\, P_{\text{drive}}\left(L,\frac{\pi}{2}\right)\frac{\mathrm{e}^{-\mathrm{j}kr_2}}{2\pi r_2}2\pi L. \qquad (57)$$

The integration along the circle of radius L will be given by Eq. (56) if $\mathrm{d}P_{\text{edge}}$ is expressed as

$$\mathrm{d}P_{\text{edge}}(r_2,\theta) = -\cos\theta\, P_{\text{drive}}\left(L,\frac{\pi}{2}\right)\frac{\mathrm{e}^{-\mathrm{j}kr_2}}{2\pi r_2}\,\mathrm{d}l. \qquad (58)$$

Finally we obtain

$$p(\mathbf{r}_2) = P_{\text{drive}}(r_2,\theta) - \cos\theta\, P_{\text{drive}}\left(L,\frac{\pi}{2}\right)\int\limits_{\text{edge}}\frac{\mathrm{e}^{-\mathrm{j}kr_P}}{2\pi r_P}\,\mathrm{d}l. \qquad (59)$$

In the final integral we changed r_2 into r_P, which is the distance from the edge element to the observation point, defined by the vector $\mathbf{r}_2$. This is acceptable provided that the observation point is far away and the angle of observation is close to 0°.

This formula defines the DED model, namely, a driving pressure with a term $(1 + \cos\theta)/2$ [Eq. (55)] and an edge term that is excited by the driving source and corresponds to a dipole in phase opposition ($-\cos\theta$) in the illuminated zone [Eq. (58)]. The driving pressure in the DED model formulation allows us to avoid a source discontinuity at the boundary between shadowed and illuminated regions.

Although our approximations are supposed to be correct in the forward direction and at large distances only, we assume that they are valid at all angles and verify that they are correct in reproducing the experimental observations.

THE AUTHORS

M. Urban

C. Heil

C. Pignon

C. Combet

P. Bauman

Marcel Urban studied at the University of Orsay, Paris, France, from which he received a Ph.D. degree in experimental physics in 1973 and a Ph.D. degree in theoretical physics in 1977. He is presently director of research at the Centre National de la Recherche Scientifique (CNRS) in France. His principal area of interest is the study of high-energy cosmic rays and he conducts research in conjunction with the AUGER observatory in Argentina. Dr. Urban has been a consultant for L-ACOUSTICS since 1983.

●

Christian Heil graduated from the University of Science of Orsay, Paris, France. He obtained a Ph.D. degree in physics in 1981, while in the department of Elementary Particles, under the direction of Dr. Urban.

He then joined Thomson Laboratories for a three-year research program on plasma physics. He also became increasingly involved in professional audio consulting, working for various corporations in the area of loudspeaker design. In 1984, Dr. Heil founded L-ACOUSTICS, where he is currently both chairman and director of R&D.

●

Christophe Pignon obtained a master's degree in signal processing and analysis from the Institut National Polytechnique of Grenoble (INPG), France, in 1991. He has worked as a research and development engineer at L-ACOUSTICS since 1995.

Christophe Combet received a master's degree in fundamental physics with a DESS specialization in computing and electronics from the Orsay University of Science, France, in 2002. He has worked in live sound reinforcement and studio recording since 2000 and has been a musician for 10 years. He joined L-ACOUSTICS as a product design engineer in 2002.

●

Paul Bauman obtained a master's degree in physics from the University of Waterloo, Ontario, Canada, in 1985 and a master's degree in electrical engineering from the McMaster University in 1991. Over the past 20 years his professional audio activities have included loudspeaker design, measurement and manufacturing, sound reinforcement system design, live sound reinforcement system engineering and FOH mixing, live and studio recording, broadcast, and performing musician. Mr. Bauman is currently director of technical support at L-ACOUSTICS, where he specializes in sound reinforcement for touring and fixed installation.

Mr. Bauman was the AES Toronto Section secretary (1986–1990); secretary for the AES 7th International Conference, Toronto, Canada, in 1989; and workshop chair for the AES 108th Convention, Paris, France, in 2000. He is currently a member of the AES Technical Committee on Acoustics and Sound Reinforcement.